PAPER

Light scattering by plasmonic disks and holes arrays: different or the same?

Light scattering by plasmonic disks and holes arrays: different or the same?

Ilia L Rasskazov[1,*] ⓘ**, Nishikant Sonwalkar**[2] **and P Scott Carney**[1]

[1] The Institute of Optics, University of Rochester, Rochester, NY 14627, United States of America
[2] SunDensity Inc., Rochester, NY 14604, United States of America

E-mail: irasskaz@ur.rochester.edu

CrossMark

Abstract
We suggest a strategy for designing regular 2D arrays of nanoholes (NHs) in metal films with far-field scattering properties similar to that of regular 2D arrays of nanodisks (NDs) with the same periodicity. Full-wave simulations for perfectly conducting, Ag and Au NDs and respectively designed arrays of NHs demonstrate a minor difference between far-field properties either at wavelengths corresponding to Wood–Rayleigh anomalies of the arrays or in a broad wavelength range, depending on the array periodicity and sizes of NDs (NHs). Our results have broad implications in plasmon-enhanced-driven applications, including optoelectronic and photovoltaic devices, where the NH arrays are preferable to be fabricated for nano-structured optics.

Keywords: scattering, plasmonic, arrays, nanoholes, nanodisks

(Some figures may appear in colour only in the online journal)

1. Introduction

Since the observation of extraordinary optical transmission in arrays of holes in Ag films [1] and its further theoretical [2] and experimental [3] elaboration, regular plasmonic nanostructures exhibiting resonant optical properties have been at the forefront of modern photonics. Arrays of *nanoholes* (NHs) in metal films, easily manufactured via focused ion beam milling [4, 5], soft interference lithography [6], ion-beam planarization [7] or direct laser writing [8], have been employed in sensing [9–16], upconversion luminescence [17], lasing [18–20], focusing [5], photocatalysis [21], thermoplasmonics [22, 23], filtering [24, 25], nonlinear optics [26], hybrid [27] and plasmon-exciton [28] coupling. One of the major drawback of NH arrays from the theoretical point of view is the lack of closed-form analytical solutions for electromagnetic properties of such nanostructures: straightforward treatment only exists for single NHs [29–32] or for NH arrays perforated in perfect electric conductor (PEC) thin films. In the

latter case, upon using analytical solutions for complementary (i.e. with the same diameter) PEC disks [33–35] and implementing the Babinet's principle, one can interchange transmittance and reflectance of disks and holes arrays: $T_d \leftrightarrow R_h$ and $R_d \leftrightarrow T_h$. For realistic materials with losses, one inevitably (except for the case of a single NH [36]) has to invoke time-consuming full-field methods and brute-force simulations to get optical properties of NHs perforated in metal films, which does not provide almost any insights into the underlying physics. Nonetheless, the Babinet principle has inspired a number of works [4, 37–41] where complementary structures of various configurations (holes/disks and far beyond) have been designed with almost perfectly complementary electromagnetic properties. Moreover, so-called 'Babinet-type' metasurfaces with a simultaneous use of complementary holes and disks have been suggested for cancelling out absorption and increasing reflectance [42] or for highly tunable transmittance [43, 44].

Unlike NHs, optical properties of regular arrays of metal *nanoparticles* of different shapes (disks, spheres, hemispheres, cones, pillars, mushrooms, crescents etc) can be intuitively understood via closed-form analytical solutions [45]. For

instance, optical properties of a single nanoparticle of almost any shape can be nearly perfectly described within the framework of the modified long-wavelength approximation (MLWA) [46–51] which, being combined with the coupled dipole approximation [52, 53], yield in results perfectly fitting both full-wave simulations and experiments [54].

Seminal comparative 'nanodisks↔nanoholes' scenario typically invokes the Babinet's principle, and the main focus is usually on complementary designed (disks and holes of the same size) nanostructures with complementary optical properties ($T_d \approx R_h$ and $R_d \approx T_h$). However, in this work we are interested in 'nanodisks↔nanoholes' scenario, where these arrays exhibit *similar* properties: $T_d \approx T_h$ and $R_d \approx R_h$. The motivation behind this interest is to bridge the gap between nanostructures composed of NHs and nanoparticles. Indeed, with existing simple and intuitively clear analytical solutions for transmission, reflectance and absorption for nanoparticles, a direct leap to NHs arrays with almost exactly the same properties may potentially facilitate a broader utilization of NHs arrays and may serve as a useful design tool for their fabrication. In what follows, we develop a strategy for designing arrays of NHs with optical properties similar to that of nanodisks (NDs) in a broadband region, with almost exact matches at wavelengths corresponding to Wood–Rayleigh anomalies (WRAs) [55, 56] of arrays.

2. Results and discussion

Consider a regular 2D square array of metal NDs with diameter D_d and height H arranged in a square lattice with pitch P, as shown in figure 1(a). We suggest to design arrays of NHs with diameter D_h and with the same pitch P as shown in figure 1(c). Rather than follow the Babinet's principle (i.e. setting $D_d = D_h$), we engineer circular cavities in the *interparticle space* as shown in figure 1(b). Having in mind a goal of designing array of NHs with electromagnetic properties similar to array of NDs, we aim to replace the most possible inter-particle space via circular cavities (figure 1(b)). NHs in a complementary array thus have a diameter (figure 1(c)):

$$D_h = \sqrt{2}P - D_d. \tag{1}$$

It is important to note that a complementary array of NHs will necessarily have similar pitch, P, as the initial array of NDs, thus the spectral position of WRAs for normal incidence, given by,

$$\lambda_{p,q} = n\frac{P}{\sqrt{p^2+q^2}}, \tag{2}$$

are preserved to maintain major resonant features inherent to the array. Here n is the refractive index of the medium surrounding the nanoparticles, and p and q are integers corresponding to the orders of diffraction in orthogonal directions within the plane of array. Integers p and q are interchangeable for square arrays considered in this work, i.e. $\lambda_{p,q} = \lambda_{q,p}$. Notice, in a half space geometry, two sets of WRAs emerge: in the substrate and in the superstrate with respective values of the refractive index, n, used in equation (2).

Figure 2 demonstrates the values of hole diameter, D_h as a function of disk diameter, D_d, and P/D_d ratio, according to equation (1). There are two specific regimes worth more careful consideration:

(i) disks and holes with a same diameter ($D_h = D_d$), which is usually examined in 'disks or holes' comparative studies [4]. In this case, $D_d = D_h = \sqrt{2}P/2$;

(ii) touching holes, i.e. $D_h = P$, which occurs if $D_d = (\sqrt{2}-1)P$. This regime is of specific interest, since the surface area covered with metal is almost the same for both NDs and NHs arrays (see figure 2(b)).

In what follows, we set the diameter and height of disks to $D_d = 300$ nm and $H = 30$ nm, respectively, and vary pitches and hole sizes accordingly, as shown in table 1.

We examine optical properties of regular arrays of PEC, Au and Ag NDs and complementary arrays of NHs in thin film with three different configurations of the host medium: (i) air host with $n = 1$, (ii) glass host with $n = 1.51$, and (iii) air-glass half-space. The reflectance and transmittance spectra of the nanostructures are calculated with the commercial Finite-Difference Time-Domain package [57]. Nanostructures are illuminated by a plane wave with normal incidence (along z axis) and polarization along x axis (figure 1). In the 'air-glass' case, the incident illumination is from the glass side. Perfectly matched layer boundary conditions are used on the top and bottom sides, while the periodic boundary conditions are applied at the lateral boundaries of the simulation box. Utilized boundary conditions imply that reflectance and transmittance spectra for NDs and NHs are normalized to the surface area of the unit cell, i.e. P^2, which is always necessarily the same for any particular NH-ND pair, as has been discussed earlier. An adaptive mesh is used to reproduce accurately the ND and NH shapes. Tabulated values [58] of dielectric constants of Ag and Au are used in simulations, while PEC is modeled as material with infinitely large dielectric constant, i.e. electric field within PEC is set to zero.

In the first conventional case with $D_h = D_d$, a clear manifestation of the Babinet's principle can be observed for PEC arrays in a homogeneous environment (figure 3). Due to relatively large absolute values of the real part of dielectric permittivity of Ag and Au for visible and near-IR wavelengths [58], these materials behave almost like PEC (the difference is solely due to the wavelength-dependence of Ag and Au permittivities), which also leads to a pronounced manifestation of the Babinet's principle: $T_h \approx R_d$ and $T_d \approx R_h$ at $\lambda \geqslant 600$ nm for arrays in air and at $\lambda \geqslant 900$ for arrays in glass (figures 4 and 5). Moreover, reflectance and transmittance spectra are almost similar for Ag and Au in the above mentioned long-wavelength region. At the same time, because the absolute value of the real part of dielectric permittivity of Ag and Au at $\lambda \leqslant 600$ nm in air and at $\lambda \leqslant 900$ in glass is ≈ 1, there is quite a discrepancy between $T_h(T_d)$ and $R_d(R_h)$ in figures 4 and 5, because Ag and Au do not behave as PEC under such conditions. Optical properties of arrays in air-glass half-space in general are more complex and resemble a mix of air
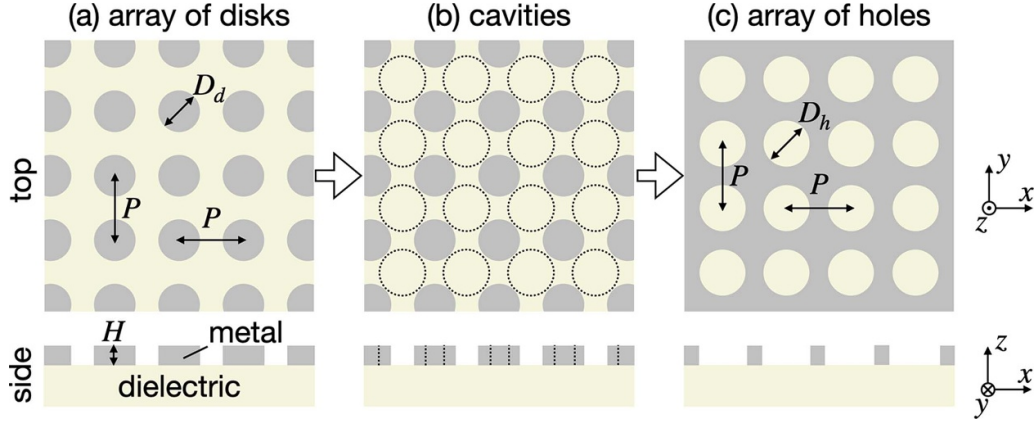
Figure 1. Design of complementary arrays of NHs: (a) initial arrays of NDs with diameter D_d arranged in a square lattice with a pitch P; (b) identification of circular interparticle cavities to be replaced with NHs; (c) complementary square array of circular NHs with diameter $D_h = \sqrt{2}P - D_d$. Arrays of disks and holes have the same pitch, P, thus spectral positions of WRAs are the same in both cases.
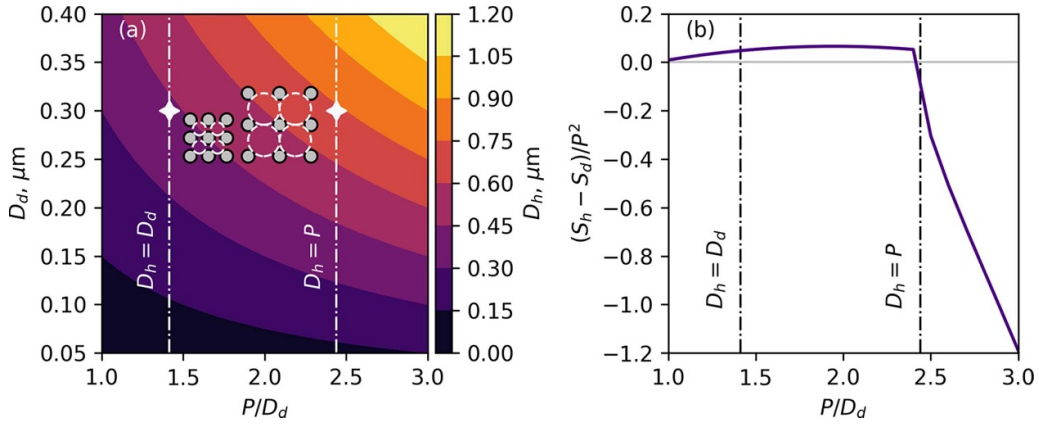
Figure 2. (a) Diameter, D_h, of complementary holes as a function of disk diameter, D_d, and normalized pitch, P/D_d, according to equation (1). (b) Normalized (per surface area of the unit cell P^2) difference between surface area occupied by metal in arrays of holes, S_h, and disks, S_d. Vertical dashed lines in (a) and (b) correspond to two specific cases: (i) holes with the diameter equal to the diameter of disks, $D_h = D_d$, and (ii) touching holes with the diameter equal to pitch, $D_h = P$. Stars in (a) correspond to configurations considered in figures 3–8 with parameters outlined in table 1.

Table 1. Parameters used for arrays of NHs and NDs considered in figures 3–8.

	$D_h = D_d$ (figures 3–5)	$D_h = P$ (figures 6–8)
D_d, nm	300	300
H, nm	30	30
P, nm	424	724
D_h, nm	300	724

and glass homogeneous environments. Interestingly, transmission and reflectance are nearly the same for disks and holes at $\lambda_{\pm1,0}^{\text{glass}} = 640$ nm in air-glass half-space for all considered materials (figures 3–5(c) and (f)). It can be explained by the similarly strong resonant interaction between NDs (NHs) at wavelengths corresponding to WRAs, which leads to almost the same respective far-field characteristics for NDs and NHs. We remind here that even though we have considered a conventional *complementary* $D_h = D_d$ case, we have chosen a specific value of period P to satisfy equation (1), which resulted

in an unexpected observation. Instead of the manifestation of the Babinet's principle (i.e. $T_d \approx R_h$ and $R_d \approx T_h$), our particular design of holes yields in counter-intuitive $T_d \approx T_h$ and $R_d \approx R_h$ cases in a half-space geometry at wavelengths corresponding to WRAs. Finally, it is also important to notice that broad peaks at $\lambda \approx 870$ nm in figures 4 and 5 are nothing but familiar localized surface plasmon resonances, which is consistent with the experimental data [59].

Another $D_h = P$ regime predictably violates the Babinet's principle, which is observed from transmission and reflection spectra in figures 6–8. However, now a distinction between optical properties of NHs and NDs surprisingly becomes less pronounced. It can be explained by the fact that for sufficiently large P, most of the interparticle space can be occupied by circular holes, which makes arrays of disks and holes almost perfectly mutually interchangeable. In other words, the surface area occupied by metal is nearly the same for arrays of NHs and NDs (cf figure 2(b)), although the shape of 'leftover particles' in between NHs is more complex than the shape of NDs. At non-resonant wavelengths below the lowest-order
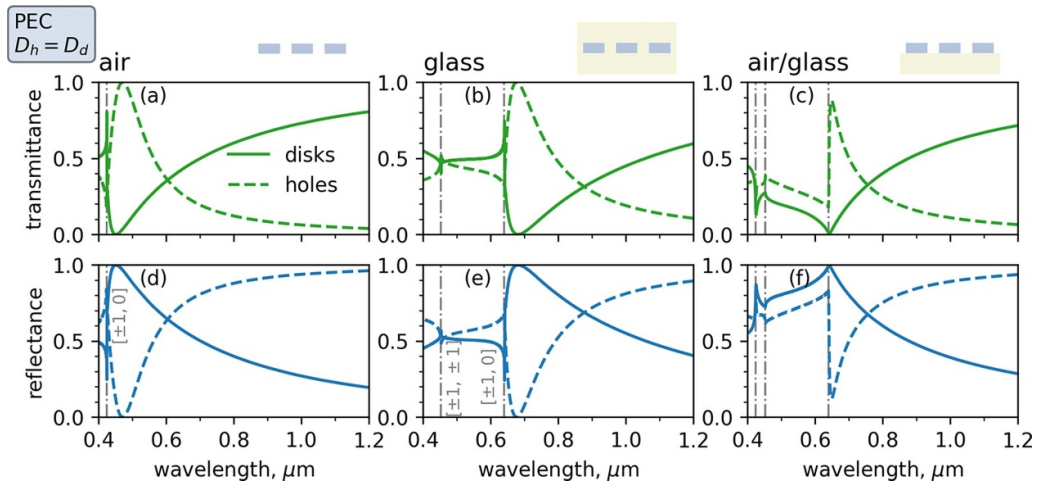
Figure 3. Transmittance and reflectance spectra for square arrays of PEC disks (solid lines) and for arrays of holes (dashed lines) for $D_h = D_d$ case. Grey vertical lines show the spectral positions of the WRAs, $\lambda_{p,q}$, in air and glass. The combined set of WRAs (both for air and glass media) is shown for air-glass configuration.
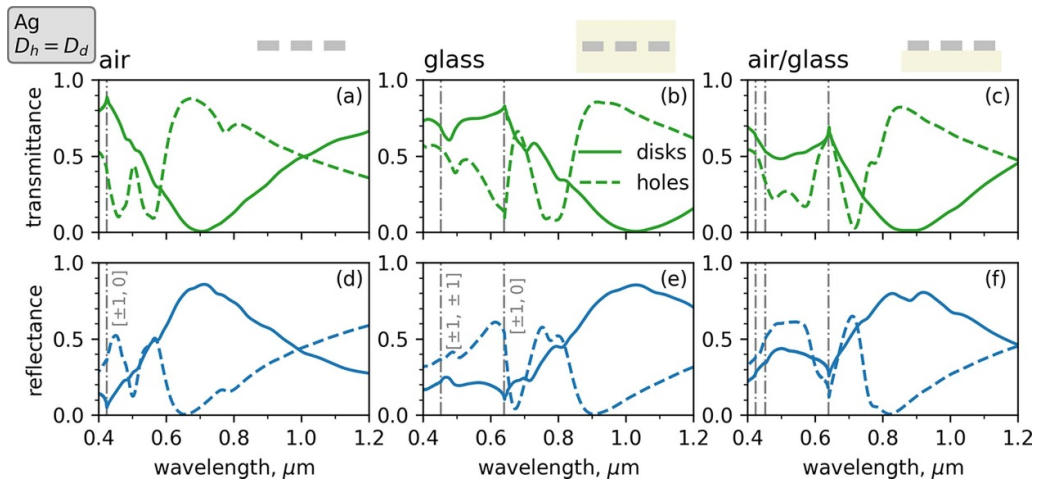
Figure 4. Same as in figure 3, but for Ag NDs and NHs in Ag thin films.

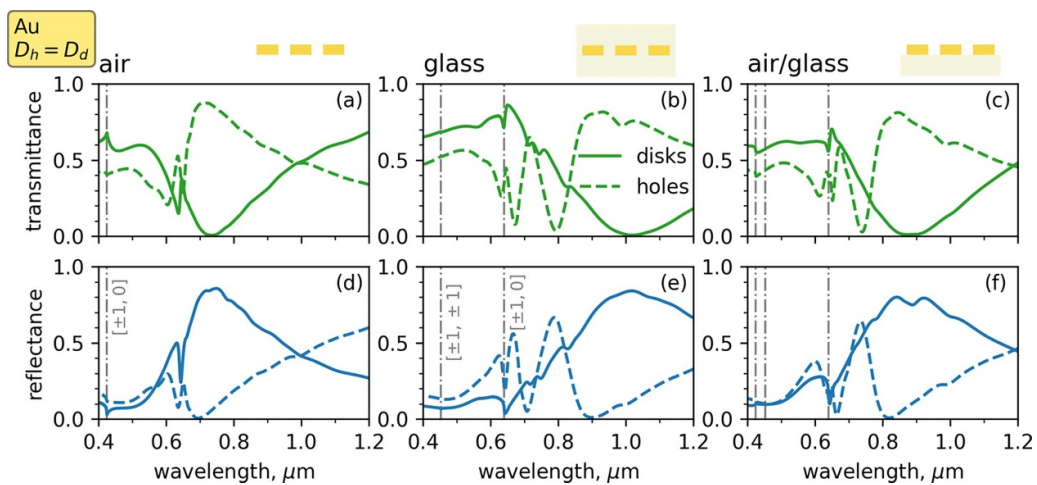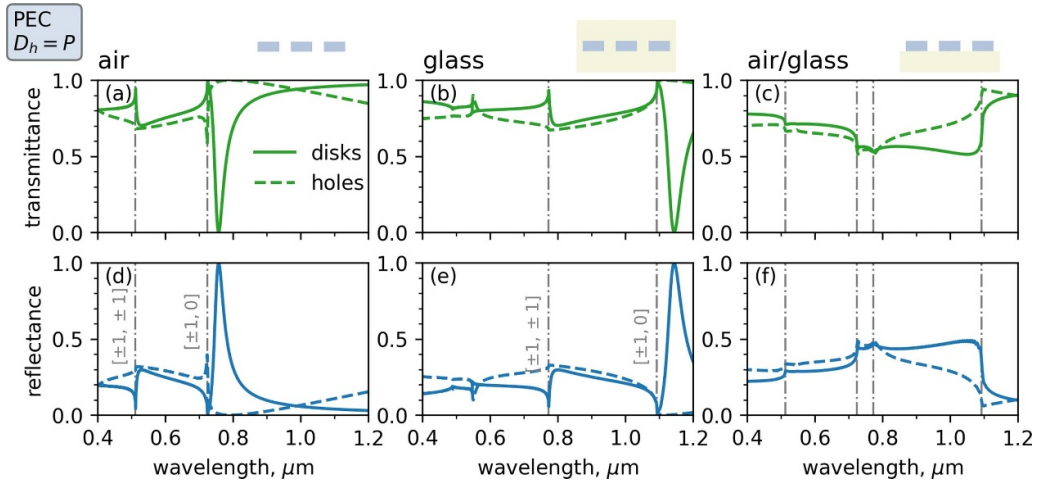**Figure 5.** Same as in figure 3, but for Au NDs and NHs in Au thin films.

Figure 6. Transmittance and reflectance spectra for square arrays of disks (solid lines) and complementary arrays of holes (dashed lines) for complementary $D_h = P$ case. Grey vertical lines show the spectral positions of the WRAs, $\lambda_{p,q}$, in air and glass. The combined set of WRAs (both for air and glass media) is shown for air-glass configuration.
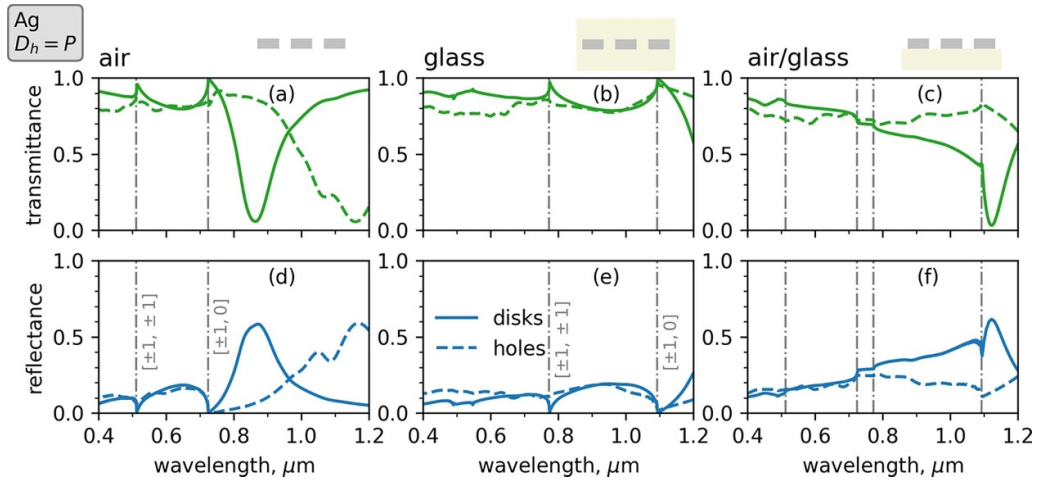

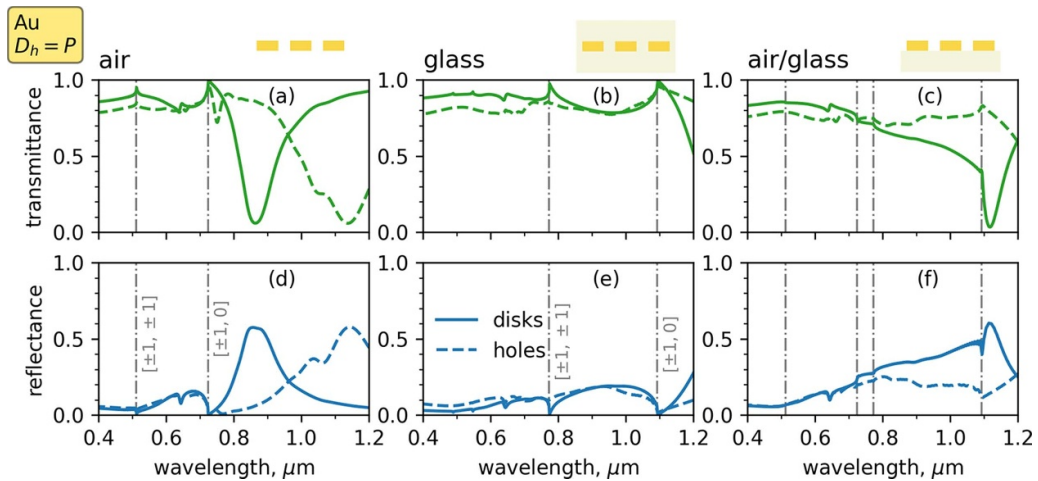**Figure 7.** The same as in figure 6, but for Ag NDs and NHs in Ag thin films.

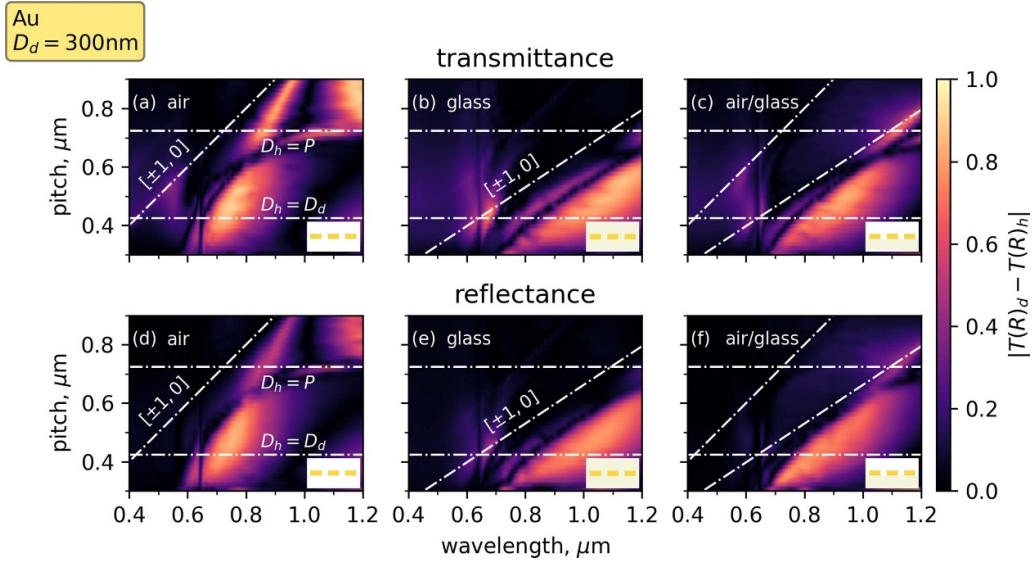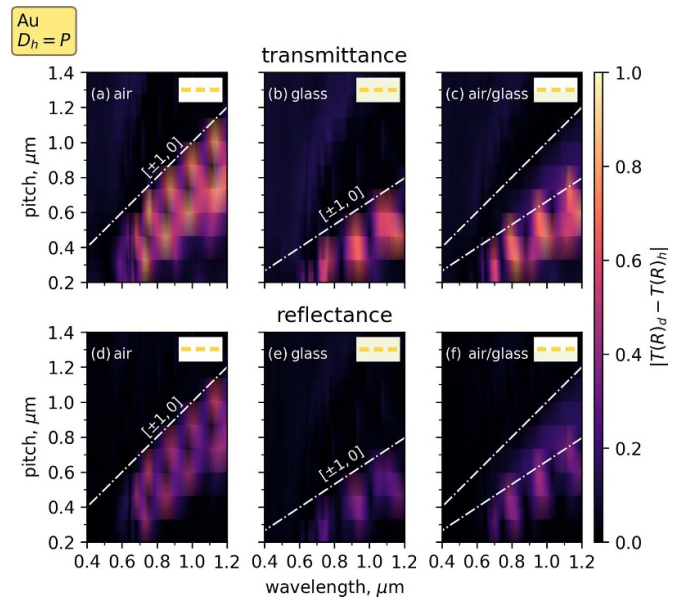**Figure 8.** The same as in figure 6, but for Au NDs and NHs in Au thin films.

Figure 9. Wavelength-dependent absolute difference between (a)–(c) transmittance and (d)–(f) reflectance of Au NDs and NHs arrays for various values of pitch P and for fixed $D_d = 300$ nm. Pitch P and NHs diameter D_h are varied to satisfy equation (1). Horizontal lines correspond to $D_h = D_d$ ($P = 424$ nm) and $D_h = P$ ($P = 724$ nm) regimes shown in details in figures 5 and 8, respectively.

WRA, $\lambda < \lambda_{\pm 1,0}$, transmittance and reflectance of disks and holes arrays are almost indistinguishable between each other, which is clearly observed for all materials considered here, even in the case of half-space geometry, where the WRA corresponding to the medium with the lowest refractive index sets the threshold for the similarity between NHs and NDs. We allude here that within this non-resonant regime, polarizabilities of NDs and 'leftover particles' are well-described via MLWA, and are only dependent on the *volume* of particles, which is a priopri the same for arrays of NDs and NHs. On the other hand, at wavelengths larger than the lowest-order WRA, $\lambda > \lambda_{\pm 1,0}$, there is a strong coherent interaction between NDs (NHs) in array which leads to the manifestation of so-called hybrid collective lattice resonances (CLRs) [60], clearly observed at $\lambda \approx \lambda_{\pm 1,0}$ in figures 6–8 (notice pronounced Fano shapes of respective resonances, inherent for CLRs). Thus, the wavelength $\lambda_{\pm 1,0}$ can be treated as the threshold wavelength distinguishing the regime with dominating non-coherent *individual* response of NDs (NHs) for $\lambda < \lambda_{\pm 1,0}$ and the regime of dominating coherent *collective* response of NDs (NHs).

A detailed illustration of the transition from complementary ($D_h = D_d$) to identical ($D_h = P$) regime is demonstrated in figure 9 for Au. An absolute difference between transmittance (reflectance) of NDs and NHs arrays gradually decreases with an increasing pitch P. In fact, the regime $D_h = P$ clearly sets the transition at which far-field properties of NHs and NDs are almost the same at $\lambda < \lambda_{\pm 1,0}$ for larger pitches. Finally, to ensure that results in figures 6–8 are not a mere luck, we performed a parametric scan for spectral properties of Au arrays with a wide range of D_d, D_h and P for $D_h = P$ condition satisfying equation (1). Figure 10 shows an absolute difference between transmittance (reflectance) of NDs and NHs arrays. It can be seen that indeed, transmittance (reflectance) becomes almost the same for arrays of NDs and NHs at wavelengths

Figure 10. Wavelength-dependent absolute difference between (a)–(c) transmittance and (d)–(f) reflectance of Au NDs and NHs arrays for various values of pitch P. Sizes of NDs and NHs are chosen to satisfy equation (1) and $D_h = P$ condition. Diameter of NDs vary from $D_d = 82$ nm for $P = 200$ nm up to $D_d = 580$ nm for $P = 1400$ nm.

starting from lowest-order WRA and below, in a homogeneous environment and in a half-space geometry.

3. Conclusion

To conclude, we have suggested an intuitive and simple approach for designing regular arrays of NHs complementary

J. Phys. D: Appl. Phys. **55** (2022) 455104

I L Rasskazov *et al*

to widely used arrays of NDs. Respective periodic structures with parameters obeying $D_h = \sqrt{2}P - D_d$ and $D_h = P$ conditions demonstrate almost similar far-field properties, which may serve as a useful guide for the design of arrays of NHs for various applications including but not limiting to sensing [9–16], upconversion luminescence [17], lasing [18–20], focusing [5], photocatalysis [21], thermoplasmonics [22, 23], filtering [24, 25], hybrid [27] and plasmon-exciton [28] coupling, and nonlinear optics [26]. Respective comparison of near-field properties [48, 61, 62] of NHs and NDs designed using this strategy are the subject of further comprehensive study. We notice that a broadband close-to-unity transmission for arrays of holes (figures 7 and 8) along with inherently efficient near-field enhancement makes them especially attractive for photovoltaic applications [63, 64]. We anticipate that disorder [65–67] or finite-size [67–69] effects will have a similar impact on optical properties of NHs arrays designed in this work as to originally studied nanoparticles.

In this work, we have limited our discussion to regular square arrays of NHs and NDs under normal illumination involving several the most representative plasmonic materials (Au and Ag) and PEC. Non-normal incidence, different lattice arrangements, other plasmonic materials and nanoparticles shapes require further examination. For instance, spectral position of localized surface plasmon resonances can be tuned upon using nanoparticles or NHs of other shapes (cubes, bars, triangles etc) [70] or other plasmonic materials: Al [71, 72], Mg [73], transparent conducting oxides (Al:ZnO, Ga:ZnO) [74, 75], and transition-metal nitrides (TiN, ZrN) [75, 76]. At the same time, spectral positions of WRAs are known to be dependent on the angle of illumination [77] and on the lattice arrangements [78]. Variety of different possible scenarios emerging from this design freedom have far-reaching consequences and ramifications for the nanoscale manufacturing of holes arrays.

Data availability statement

All data that support the findings of this study are included within the article (and any supplementary files).

Funding

Conflict of interest

The authors declare no conflicts of interest.

ORCID iD

Ilia L Rasskazov https://orcid.org/0000-0002-7956-1702

References

[1] Ebbesen T W, Lezec H J, Ghaemi H F, Thio T and Wolff P A 1998 Extraordinary optical transmission through sub-wavelength hole arrays *Nature* **391** 667–9

[2] Ghaemi H F, Thio T, Grupp D E, Ebbesen T W and Lezec H J 1998 Ebbesen T W and Lezec H J Surface plasmons enhance optical transmission through subwavelength holes *Phys. Rev.* B **58** 6779–82

[3] Schröter U and Heitmann D 1998 Surface-plasmon-enhanced transmission through metallic gratings *Phys. Rev.* B **58** 15419–21

[4] Parsons J, Hendry E, Burrows C P, Auguié B, Sambles J R and Barnes W L 2009 Localized surface-plasmon resonances in periodic nondiffracting metallic nanoparticle and nanohole arrays *Phys. Rev.* B **79** 073412

[5] Gao H, Hyun J K, Lee M H, Yang J C, Lauhon L J and Odom T W 2010 Broadband plasmonic microlenses based on patches of nanoholes *Nano Lett.* **10** 4111–6

[6] Henzie J, Lee M H and Odom T W 2007 Multiscale patterning of plasmonic metamaterials *Nat. Nanotechnol.* **2** 549–54

[7] Liu Q, Song Y, Zeng P, Zhang C, Chen Y, Wang H, Luo Y and Duan H 2020 High-fidelity fabrication of plasmonic nanoholes array via ion-beam planarization for extraordinary transmission applications *Appl. Surf. Sci.* **526** 146690

[8] Mao F, Ngo G L, Nguyen C T, Ledoux-Rak I and Lai N D 2021 Direct fabrication and characterization of gold nanohole arrays *Opt. Express* **29** 29841–56

[9] McMahon J M, Henzie J, Odom T W, Schatz G C and Gray S K 2007 Tailoring the sensing capabilities of nanohole arrays in gold films with Rayleigh anomaly-surface plasmon polaritons *Opt. Express* **15** 18119–29

[10] Gordon R, Sinton D, Kavanagh K L and Brolo A G 2008 A new generation of sensors based on extraordinary optical transmission *Acc. Chem. Res.* **41** 1049–57

[11] Eftekhari F, Escobedo C, Ferreira J, Duan X, Girotto E M, Brolo A G, Gordon R and Sinton D 2009 Nanoholes as nanochannels: flow-through plasmonic sensing *Anal. Chem.* **81** 4308–11

[12] Yanik A A, Huang M, Kamohara O, Artar A, Geisbert T W, Connor J H and Altug H 2010 An optofluidic nanoplasmonic biosensor for direct detection of live viruses from biological media *Nano Lett.* **10** 4962–9

[13] Yanik A A, Cetin A E, Huang M, Artar A, Mousavi S H, Khanikaev A, Connor J H, Shvets G and Altug H 2011 Seeing protein monolayers with naked eye through plasmonic Fano resonances *Proc. Natl Acad. Sci.* **108** 11784–9

[14] Eitan M, Iluz Z, Yifat Y, Boag A, Hanein Y and Scheuer J 2015 Degeneracy breaking of Wood's anomaly for enhanced refractive index sensing *ACS Photon.* **2** 615–21

[15] Larson S, Carlson D, Ai B and Zhao Y 2019 The extraordinary optical transmission and sensing properties of Ag/Ti composite nanohole arrays *Phys. Chem. Chem. Phys.* **21** 3771–80

[16] Sanders S, Dowran M, Jain U, Lu T M, Marino A M and Manjavacas A 2022 Lattice resonances of nanohole arrays for quantum enhanced sensing *Phys. Rev. Appl.* **17** 014035

[17] Saboktakin M, Ye X, Chettiar U K, Engheta N, Murray C B and Kagan C R 2013 Plasmonic enhancement of nanophosphor upconversion luminescence in Au nanohole arrays *ACS Nano* **7** 7186–92

[18] van Beijnum F, van Veldhoven P J, Geluk E J, de Dood M J A, 't Hooft G W and van Exter M P 2013 Surface plasmon lasing observed in metal hole arrays *Phys. Rev. Lett.* **110** 206802

J. Phys. D: Appl. Phys. **55** (2022) 455104

I L Rasskazov *et al*

[19] Krause B, Pham M T, Luong H M, Nguyen T D and Hoang T B 2022 Periodic nanohole arrays with enhanced lasing and spontaneous emissions for low-cost plasmonic devices *ACS Appl. Nano Mater.* **5** 1185–91

[20] Mendoza-Sandoval E, Rodríguez-López G, Ordíñez-Romero C L, Ley D, Qureshi N, Urbánek M, Solis-Ibarra D, Noguez C, Lara-García H A and Pirruccio G 2022 Shaping and enhancing the photoluminescence of halide perovskite quantum dots with plasmonic lattices *J. Mater. Chem.* C **10** 3704–11

[21] Ai B, Wang Z, Möhwald H and Zhang G 2017 Plasmonic nanochemistry based on nanohole array *ACS Nano* **11** 12094–102

[22] Virk M, Xiong K, Svedendahl M, Käll M and Dahlin A B 2014 A thermal plasmonic sensor platform: resistive heating of nanohole arrays *Nano Lett.* **14** 3544–9

[23] Tordera D, Zhao D, Volkov A V, Crispin X and Jonsson M P 2017 Thermoplasmonic semitransparent nanohole electrodes *Nano Lett.* **17** 3145–51

[24] Shah Y D, Grant J, Hao D, Kenney M, Pusino V and Cumming D R S 2018 Ultra-narrow line width polarization-insensitive filter using a symmetry-breaking selective plasmonic metasurface *ACS Photon.* **5** 663–9

[25] Shafagh S G, Kaatuzian H and Danaie M 2021 Design and analysis of infrared tunable all-optical filters based on plasmonic hybrid nanostructure using periodic nanohole arrays *Plasmonics* **17** 693–708

[26] You J W, Lan Z and Panoiu N C 2020 Four-wave mixing of topological edge plasmons in graphene metasurfaces *Sci. Adv.* **6** eaaz3910

[27] Vázquez-Guardado A, Safaei A, Modak S, Franklin D and Chanda D 2014 Hybrid coupling mechanism in a system supporting high order diffraction, plasmonic and cavity resonances *Phys. Rev. Lett.* **113** 263902

[28] Kang E S H, Chen S, Sardar S, Tordera D, Armakavicius N, Darakchieva V, Shegai T and Jonsson M P 2018 Strong plasmon-exciton coupling with directional absorption features in optically thin hybrid nanohole metasurfaces *ACS Photon.* **5** 4046–55

[29] Bethe H A 1944 Theory of diffraction by small holes *Phys. Rev.* **66** 163–82

[30] Levine H and Schwinger J 1948 On the theory of diffraction by an aperture in an infinite plane screen. I *Phys. Rev.* **74** 958–74

[31] Levine H and Schwinger J 1949 On the theory of diffraction by an aperture in an infinite plane screen. II *Phys. Rev.* **75** 1423–32

[32] Levine H and Schwinger J 1950 On the theory of electromagnetic wave diffraction by an aperture in an infinite plane conducting screen *Commun. Pure Appl. Math.* **3** 355–91

[33] García de Abajo F J, Gómez-Medina R and Sáenz J J 2005 Full transmission through perfect-conductor subwavelength hole arrays *Phys. Rev.* E **72** 016608

[34] García de Abajo F J 2007 Colloquium: light scattering by particle and hole arrays *Rev. Mod. Phys.* **79** 1267–90

[35] Bass S F and Ruyle J E 2019 Adaptation of Babinet's principle for complementary antennas in a dielectric half-space *IEEE Antennas Wirel. Propag. Lett.* **18** 333–7

[36] Horing N J M, Miessein D and Gumbs G 2015 Electromagnetic wave transmission through a subwavelength nano-hole in a two-dimensional plasmonic layer *J. Opt. Soc. Am.* A **32** 1184–98

[37] Falcone F, Lopetegi T, Laso M A, Baena J D, Bonache J, Beruete M, Marques R, Martín F and Sorolla M 2004 Babinet principle applied to the design of metasurfaces and metamaterials *Phys. Rev. Lett.* **93** 197401

[38] Chen H T, O'Hara J F, Taylor A J, Averitt R D, Highstrete C, Lee M and Padilla W J 2007 Complementary planar terahertz metamaterials *Opt. Express* **15** 1084–95

[39] Zentgraf T, Meyrath T P, Seidel A, Kaiser S, Giessen H, Rockstuhl C and Lederer F 2007 Babinet's principle for optical frequency metamaterials and nanoantennas *Phys. Rev.* B **76** 033407

[40] Hand T H, Gollub J, Sajuyigbe S, Smith D R and Cummer S A 2008 Characterization of complementary electric field coupled resonant surfaces *Appl. Phys. Lett.* **93** 212504

[41] Horák M *et al* 2019 Limits of Babinet's principle for solid and hollow plasmonic antennas *Sci. Rep.* **9** 4004

[42] Kornienko V V, Shaimanov A N and Baryshev A V 2019 Overlapping the electric and magnetic dipole resonances of a silver 2D Babinet-type metasurface: broadband high reflectance with local field enhancement *J. Appl. Phys.* **126** 063102

[43] Akinoglu G E, Akinoglu E M, Kempa K and Giersig M 2019 Plasmon resonances in coupled Babinet complementary arrays in the mid-infrared range *Opt. Express* **27** 22939–50

[44] Akinoglu G E, Akinoglu E M, Kempa K and Hutchison J A 2021 Materials design of vertically coupled plasmonic arrays *Nanoscale Adv.* **3** 6925–33

[45] Abujetas D R, Olmos-Trigo J, Sáenz J J and Sánchez-Gil J A 2020 Coupled electric and magnetic dipole formulation for planar arrays of particles: resonances and bound states in the continuum for all-dielectric metasurfaces *Phys. Rev.* B **102** 125411

[46] Meier M and Wokaun A 1983 Enhanced fields on large metal particles: dynamic depolarization *Opt. Lett.* **8** 581–3

[47] Chung H Y, Leung P T and Tsai D P 2009 Dynamic modifications of polarizability for large metallic spheroidal nanoshells *J. Chem. Phys.* **131** 124122

[48] Zorić I, Zäch M, Kasemo B and Langhammer C 2011 Gold, platinum and aluminum nanodisk plasmons: material independence, subradiance and damping mechanisms *ACS Nano* **5** 2535–46

[49] Schebarchov D, Auguié B and Le Ru E C 2013 Simple accurate approximations for the optical properties of metallic nanospheres and nanoshells *Phys. Chem. Chem. Phys.* **15** 4233–42

[50] Januar M, Liu B, Cheng J C, Hatanaka K, Misawa H, Hsiao H H and Liu K C 2020 Role of depolarization factors in the evolution of a dipolar plasmonic spectral line in the far- and near-field regimes *J. Phys. Chem.* C **124** 3250–9

[51] Rasskazov I L, Zakomirnyi V I, Utyushev A D, Carney P S and Moroz A 2021 Remarkable predictive power of the modified long wavelength approximation *J. Phys. Chem.* C **125** 1963–71

[52] Markel V 1993 Coupled-dipole approach to scattering of light from a one-dimensional periodic dipole structure *J. Mod. Opt.* **40** 2281–91

[53] Markel V A 2019 Extinction, scattering and absorption of electromagnetic waves in the coupled-dipole approximation *J. Quant. Spectrosc. Radiat. Transfer* **236** 106611

[54] Bin-Alam M S *et al* 2021 Ultra-high-Q resonances in plasmonic metasurfaces *Nat. Commun.* **12** 974

[55] Wood R W 1902 On a remarkable case of uneven distribution of light in a diffraction grating spectrum *Proc. Phys. Soc. London* **18** 269–75

[56] Rayleigh L 1907 On the dynamical theory of gratings *Proc. R. Soc.* A **79** 399–416

[57] Lumerical Solutions *FDTD Solutions* (available at: www.lumerical.com/tcad-products/fdtd/) (Accessed 7 September 2022)

[58] Palik E D 1998 *Handbook of Optical Constants of Solids II* (New York: Academic)

[59] Zheng Y B, Juluri B K, Mao X, Walker T R and Huang T J 2008 Systematic investigation of localized surface plasmon

J. Phys. D: Appl. Phys. **55** (2022) 455104

I L Rasskazov *et al*

resonance of long-range ordered Au nanodisk arrays *J. Appl. Phys.* **103** 014308

[60] Utyushev A D, Zakomirnyi V I and Rasskazov I L 2021 Collective lattice resonances: plasmonics and beyond *Rev. Phys.* **6** 100051

[61] Rechberger W, Hohenau A, Leitner A, Krenn J, Lamprecht B and Aussenegg F 2003 Optical properties of two interacting gold nanoparticles *Opt. Commun.* **220** 137–41

[62] Qin F, Cui X, Ruan Q, Lai Y, Wang J, Ma H and Lin H Q 2016 Role of shape in substrate-induced plasmonic shift and mode uncovering on gold nanocrystals *Nanoscale* **8** 17645–57

[63] Menezes J W, Ferreira J, Santos M J L, Cescato L and Brolo A G 2010 Large-area fabrication of periodic arrays of nanoholes in metal films and their application in biosensing and plasmonic-enhanced photovoltaics *Adv. Funct. Mater.* **20** 3918–24

[64] Wang Y, Sun T, Paudel T, Zhang Y, Ren Z and Kempa K 2012 Metamaterial-plasmonic absorber structure for high efficiency amorphous silicon solar cells *Nano Lett.* **12** 440–5

[65] Auguié B and Barnes W L 2009 Diffractive coupling in gold nanoparticle arrays and the effect of disorder *Opt. Lett.* **34** 401–3

[66] Zhang F, Tang F, Xu X, Adam P M, Martin J and Plain J 2020 Influence of order-to-disorder transitions on the optical properties of the aluminum plasmonic metasurface *Nanoscale* **12** 23173–82

[67] Warren A, Alkaisi M M and Moore C P 2022 Finite-size and disorder effects on 1D unipartite and bipartite surface lattice resonances *Opt. Express* **30** 3302–15

[68] Rodriguez S, Schaafsma M, Berrier A and Gómez Rivas J 2012 Collective resonances in plasmonic crystals: size matters *Physica* B **407** 4081–5

[69] Zundel L and Manjavacas A 2019 Finite-size effects on periodic arrays of nanostructures *J. Phys. Photon.* **1** 015004

[70] Xia Y and Halas N J 2005 Shape-controlled synthesis and surface plasmonic properties of metallic nanostructures *MRS Bull.* **30** 338–48

[71] Knight M W, King N S, Liu L, Everitt H O, Nordlander P and Halas N J 2014 Aluminum for plasmonics *ACS Nano* **8** 834–40

[72] Gérard D and Gray S K 2015 Aluminium plasmonics *J. Phys. D: Appl. Phys.* **48** 184001

[73] Ringe E 2020 Shapes, plasmonic properties and reactivity of magnesium nanoparticles *J. Phys. Chem.* C **124** 15665–79

[74] West P, Ishii S, Naik G, Emani N, Shalaev V and Boltasseva A 2010 Searching for better plasmonic materials *Laser Photon. Rev.* **4** 795–808

[75] Naik G V, Kim J and Boltasseva A 2011 Oxides and nitrides as alternative plasmonic materials in the optical range [Invited] *Opt. Mater. Express* **1** 1090–9

[76] Naik G V, Schroeder J L, Ni X, Kildishev A V, Sands T D and Boltasseva A 2012 Titanium nitride as a plasmonic material for visible and near-infrared wavelengths *Opt. Mater. Express* **2** 478–89

[77] Utyushev A D, Zakomirnyi V I, Ershov A E, Gerasimov V S, Karpov S V and Rasskazov I L 2020 Collective lattice resonances in all-dielectric nanostructures under oblique incidence *Photonics* **7** 24

[78] Ekşioğlu Y, Cetin A E and Petráček J 2016 Optical response of plasmonic nanohole arrays: comparison of square and hexagonal lattices *Plasmonics* **11** 851–6